COBEM 99
XV Congresso Brasileiro de Engenharia Mecânica
15th Brazilian Congress of Mechanical Engineering
22 - 26 de Novembro de 1999 / November 22 - 26, 1999 Águas de Lindóia, São Paulo,

ANALYSIS OF THE AIR FLOW BETWEEN A MOVING SUBSTRATE AND A CURVED PLATE

Márcio da S. Carvalho
Department of Mechanical Engineering
Pontifícia Universidade Católica do Rio de Janeiro
Rua Marquês de São Vicente, 225, Gávea
Rio de Janeiro, RJ, 22453-900, Brazil
William B. Kolb
Imation Corporation
1 Imation Place
Oakdale, MN, 55128-3414, USA

Abstract. *Conventional drying of coated substrates usually use air impingement to support and heat the coated web. Because of the high velocity air flow, most of the heat is transferred by convection and the heat transfer coefficient is not uniform, which can lead to drying defects. A way of overcoming this problem and obtain a high uniform heat transfer coefficient is to supply the energy to the back side of the substrate by conduction through a very thin air layer between a heated plate and the moving substrate. Therefore, it is essential to form and to be able to control a thin, uniform and stable air layer between the substrate and the heating plate. This work presents a theoretical analysis of the air flow between a moving flexible substrate and a curved solid surface. The goal is to understand this elastohydrodynamic action and determine how the air layer thickness changes with the plate geometry, substrate material and operating conditions. The theoretical model consisted of the Navier-Stokes equation to describe the air motion and cylindrical shell approximation to model the deformation of the web. The differential equations were solved by the Galerkin / finite element method. The agreement between the predicted air layer thickness and those measured experimentally was very good.*

Key words: *elastohydrodynamics, drying, finite element method.*

1. INTRODUCTION

When a flexible moving substrate is traveling over a solid surface, a thin layer of air is entrapped between the two surfaces. This case of hydrodynamic lubrication is generally referred to as foil bearing.

The control of the thickness of the air layer between two surfaces is vital in many situations. The application that motivated this work is related to the floatation of a moving substrate over hot solid surfaces inside an oven, as described next.

The conventional drying process for coated substrate usually uses the two-sided impingement dryer technology. Nozzles of varying design impinge air to both sides of the web. Air serves to support the web, and to supply heat to both the wet and the back side of

the coated substrate. Because of the high velocity air flow, most of the heat is transferred to the web by convection. The air flow is highly non-uniform and turbulent, leading to non-uniform heat transfer coefficient. This non-uniformity may lead to drying defects. Controlling the amount of energy supplied to the back side of the web is not easy. The effect of the operating parameters on the drying rate is usually determined after extensive trial and error experimentation. Moreover, the amount of air that needs to be treated for solvent recovery purpose and pollution control is usually very large. A new drying technology has been developed recently by Huelsman and Kolb (1997) to overcome these problems. It provides accurate control of heat transfer rates, eliminates the need for forced gas flow, as in the case of impingement ovens, and provides direct solvent recovery. Kolb and Hueslman (1998) discuss the advantages of this new drying method when compared to existing technologies.

In this new method, heat to evaporate the solvent is supplied to the substrate from the back side and a chilled plate is located above the web to remove the solvent by condensation, as illustrated in Fig.1. The energy is transfered from the hot plate to the back side of the substrate mainly by conduction through the air layer between the two surfaces. Therefore, the heat transfer coefficient is given by the ratio of thermal conductivity of air to the air layer thickness. To obtain large and uniform heat transfer coefficients, the air layer thickness has to be very small and constant, both in time and space.

An uniform, stable and thin air layer between a moving web and a heated plate without forced air can be obtained by using a plate with a large radius of curvature. The plate is positioned such that the web wraps part of it, as indicated in Fig.2. The moving web drags air and a thin air layer under pressure is formed between the two surfaces. The amount of air entrapped is controlled by the plate geometry, web speed and tension.

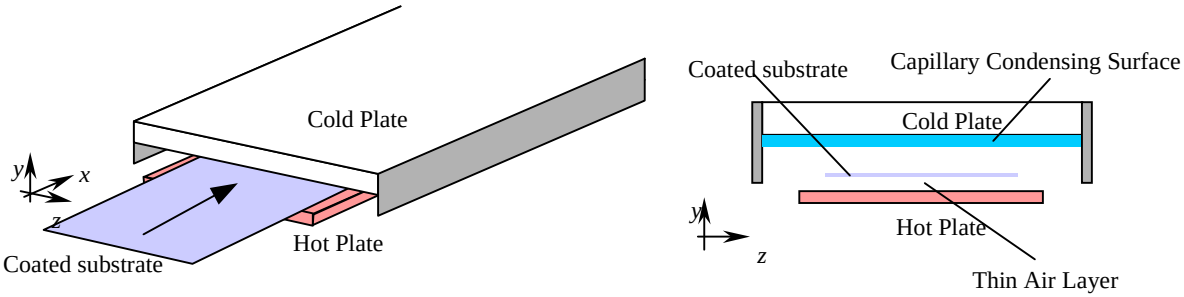

Figure 1: Schematic of the drying method proposed by Huelsman and Kolb (1997).

This work presents an analysis of the air flow between a moving web and a stationary curved solid surface. The goal is to understand how the air film thickness changes with the geometry of the plate and operating conditions. This information can be used to design plates such that the air layer thickness can be adjusted according to the drying rates required by different products.

The first analysis of foil bearing was done by Blok and Van Rossum (1953). They measured the thickness of a lubrication oil layer between a thin cellophane foil and a cylinder (radius R_0). Elshel and Elrod (1965) developed a theoretical model using Reynolds equation of lubrication to describe the fluid flow with the assumptions of incompressibility, and infinitely wide foil of negligible stiffness. The relationship between the fluid thickness H_0 and operating parameters they derived is:

$$H_0 = 0.643 R_0 \left(6 \frac{\mu V}{T} \right)^{2/3}, \qquad (1)$$

where μ is the liquid viscosity and V, the substrate velocity.

Eshel and Elrod later (1967) extended their work and analyzed the effect of foil stiffness. They showed that, for the range of parameters they explored, the stiffer the web, the smaller the air layer thickness. Licht (1968) presented an extensive experimental study of elastohydrodynamic lubrication of foil bearings. His measurements were in good agreement with the theoretical predictions of Eshel and Elrod. However, Eshel (1970) has shown that the geometry of the solid surface has a remarkable effect on the air film thickness and that Eq.(1) fails to predict the air layer thickness in situations where the geometry of the solid surface is not a cylinder, as in the case of the radius plates used in the drying method described before. In order to obtain an accurate relation between the air layer thickness, the operating conditions and the plate configuration, a complete two-dimensional model for the air flow has to be employed.

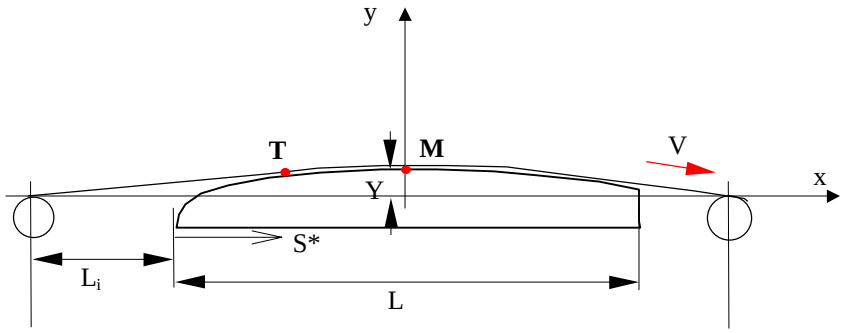

Figure 2: Geometry of a substrate moving over a curved plate. The upstream and downstream idlers are positioned such that the web wraps part of the plate.

In this work, the air motion is described by the Navier-Stokes equation and the deformation of the substrate is modeled by the cylindrical shell approximation. The air flow and web deformation are assumed to be two-dimensional, i.e., the flow and float height variation in the cross-web direction are neglected. In reality, a small amount of air escapes from beneath the web through the sides. The differential equations that describe the problem are solved by the Galerkin / Finite Element Method.

2. ELASTOHYDRODYNAMIC MODEL

2.1. Governing Equations

The configuration of the problem analyzed in this report is illustrated in Fig.2. The air dragged by the moving substrate (in the figure, the web is moving from left to right) generates pressure due to the converging channel formed between the substrate and the curved plate. The air pressure deforms the substrate. The flow and the deformation are coupled in what is called elastohydrodynamic behavior.

It is important to characterize the position of the plate relative to the upstream and downstream idler rolls that guide the moving web. The relative position can be characterized by the distance Y from the middle point M of the plate to the x-axis. When $Y < 0$, the web does not touch the plate. When $Y > 0$, the web wraps around a portion of the plate. An alternative way is by the distance from the point T, where a stationary web first touches the plate, to the upstream edge of the plate, denoted by S^*, and shown in Fig.2. Each value of Y corresponds to one value of S^*. As the plate is pushed against the web and Y increases, the tangent point T moves towards the upstream edge of the plate, and S^* decreases.

The web is assumed to be infinitely wide, and therefore the flow in the transverse direction is neglected. The motion of the air is described by the Navier-Stokes equation and continuity equation for incompressible Newtonian fluid:

$$\rho \mathbf{v}\cdot\nabla\mathbf{v} - \nabla\cdot\left[-p\mathbf{I} + \mu\left(\nabla\mathbf{v} + (\nabla\mathbf{v})^T\right)\right] = 0 \quad \text{and} \quad \nabla\cdot\mathbf{v} = 0 \tag{2}$$

together with appropriate boundary conditions. ρ and μ are the air density and viscosity, respectively. The deformation of the web is modeled by the equations of cylindrical shells:

$$\begin{aligned} &\frac{dT}{d\xi} + \kappa\frac{d}{d\xi}(\kappa D) + P_t + W_t = 0 \\ &-\frac{d^2}{d\xi^2}(\kappa D) + \kappa T + P_n + W_n = 0 \\ &\frac{d^2x}{d\xi^2} + \kappa\frac{dy}{d\xi} = 0 \quad \text{or} \quad \frac{d^2y}{d\xi^2} - \kappa\frac{dx}{d\xi} = 0. \end{aligned} \tag{3}$$

ξ is the coordinate along the web. T and κ are the web tension and curvature at each position, and x and y are the Cartesian coordinates of points on the web. The web stiffness $D \equiv Et^3/12\left(1-\upsilon^2\right)$ is a function of the Elastic Modulus E, Poisson ratio υ, and thickness of the web t. P_t and P_n are the forces on the web in the tangential and normal direction.

Figure 3 shows the domain of calculation. It is divided into two different subdomains: One where the Navier-Stokes equation is solved (Ω_f), and the other where the cylindrical shell equations are solved (Ω_s). At the plate surface, labeled (1) in Fig.3, the no-slip and no-penetration conditions apply. The artifical boundaries (2) that limit the fluid domain underneath the plate were located far enough below the plate that its location had no effect on the predictions reported here. On that position, the air is assumed to be stagnant. Along the artificial inflow and outflow (3), the pressure is assumed constant (atmospheric). The inflow and outflow plane were positioned such that the theoretical predictions were virtually insensitive to moving the boundaries further away from the plane. At the interface between the air and the flexible substrate (4), the air velocity is equal to the web velocity, and the loading force responsible for the web deformation is the traction exerted by the air. In one extreme of the substrate (5), the position, curvature and web tenstion have to be specified; in the other (6), only the position and curvature are specified.

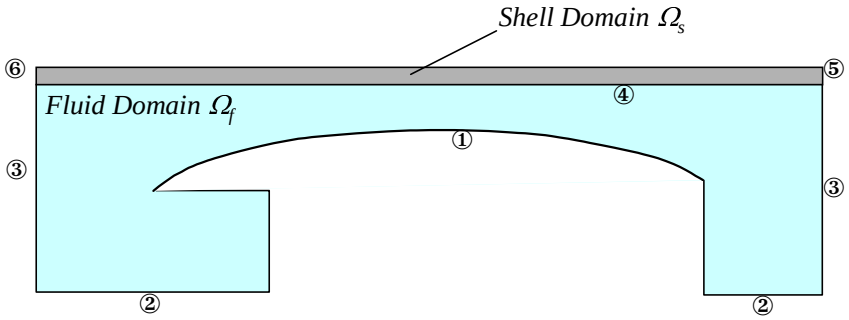

Figure 3: Domain of calculation. Ω_f is the fluid domain and Ω_s is the shell domain.

This situation is governed by the following dimensionless groups:

Reynolds Number : $\mathrm{Re} \equiv \frac{\rho V H_0}{\mu}$; Tension Number : $\tau \equiv \frac{\mu V}{T}$; Elasticity Number : $N_{ES} \equiv \frac{D}{TR_0^2} = \frac{Et^3}{12(1-\upsilon^2)TR_0^2}$; Wrapping Angle : $\alpha \equiv \frac{L_S}{R_0}$; Dimensionless Length : $\frac{L}{R_0}$.

The model presented here incorporates several simplifying assumptions. The first idealization is that the flow in the cross-web direction is neglected, i.e., the flow is assumed to be two-dimensional. In reality, because the air underneath the web is under pressure, a small amount of it escapes through the sides. The two-dimensional model also does not take into account the bagginess of the web. Another important simplification is that the mathematical formulation used to describe the situation enforces that there is always a layer of air between the web and the plate. Therefore, the theoretical calculations presented cannot predict at what conditions the web touches the plate. Nonetheless, this two-dimensional model can still capture the overall features and trends of the process. It clarifies how and why the air layer thickness is controlled by the plate geometry. Conditions at which the web touches the plate can still be estimated by using treshold limits in the air layer thickness.

2.2. Solution Method

The governing equations and the boundary conditions give rise to a free boundary problem. The location of the web is unknown a priori. The basis of treating such problems is recounted briefly here. Fuller accounts were given by Kistler and Scriven (1983), Sackinger et al. (1996), and Carvalho and Scriven (1997).

In order to solve a free boundary problem using standard techniques for boundary value problems, the set of differential equations posed in the unknown physical domain has to be transformed to an equivalent set defined in a known, fixed reference domain. This approach has been extensively used to solve viscous flow with liquid / air interface. In that class of problem, the position of the interface is implicitly located by imposing the kinematic boundary condition at the free surface. In the situation studied here, the position of the web is implicitly located by imposing the system of ordinary differential equations (3). The transformation of the set of differential equations that governs the problem is made by a mapping $\mathbf{x} = \mathbf{x}(\xi)$ that connects the physical domain, parameterized by the position vector $\mathbf{x} = (x, y)$, and the reference domain, parameterized by $\boldsymbol{\xi} = (\xi, \eta)$. The inverse of the mapping is governed by a pair of elliptic differential equations identical with those encountered in the dilute regime of diffusional transport. The coordinate potencials ξ and η satisfy

$$\nabla \cdot (D_\xi \nabla \xi) = 0 \quad \text{and} \quad \nabla \cdot (D_\eta \nabla \eta) = 0 \tag{4}$$

The Navier-Stokes equation (2), the substrate deformation (3) and the mesh generation equations (4) together with the respective boundary conditions were solved by the Galerkin / finite element method. Biquadratic basis functions were used to represent both the velocity and the mapping from the reference to the physical domain. The basis functions used to represent the pressure field were piecewise, linear and discontinuous.

The resulting non-linear system of algebraic equations for the coefficients of the basis functions were solved by Newton's method. The domain was divided into 476 elements with 8928 unknowns. The computations were performed in a HP model J-200 workstation, and each solution took approximalety 10 minutes to be computed.

In order to obtain solutions at large wrapping angles, i.e., large values of *Y*, a good initial guess is vital. The procedure adopted was to first obtain solutions with the plate far from the web, i.e., $Y < 0$. At these conditions, the pressure that builds up in the air is very small leading to small web deformation. A solution can be obtained even with a poor initial guess. After a solution is computed, a first-order, arc-length continuation on the position of the plate was used to obtain solutions at the relevant set of parameters. Figure 4 illustrates a sequence of solutions as the plate is moved upwards and pushed against the web.

3. THEORETICAL PREDICTIONS

As mentioned before, both the coordinate of the middle point of the plate Y or the position S^* of the tangent point of the web on the plate can be used to characterize the relative location of the plate and the idlers. The later is easier to measure experimentally, and for this reason is used here.

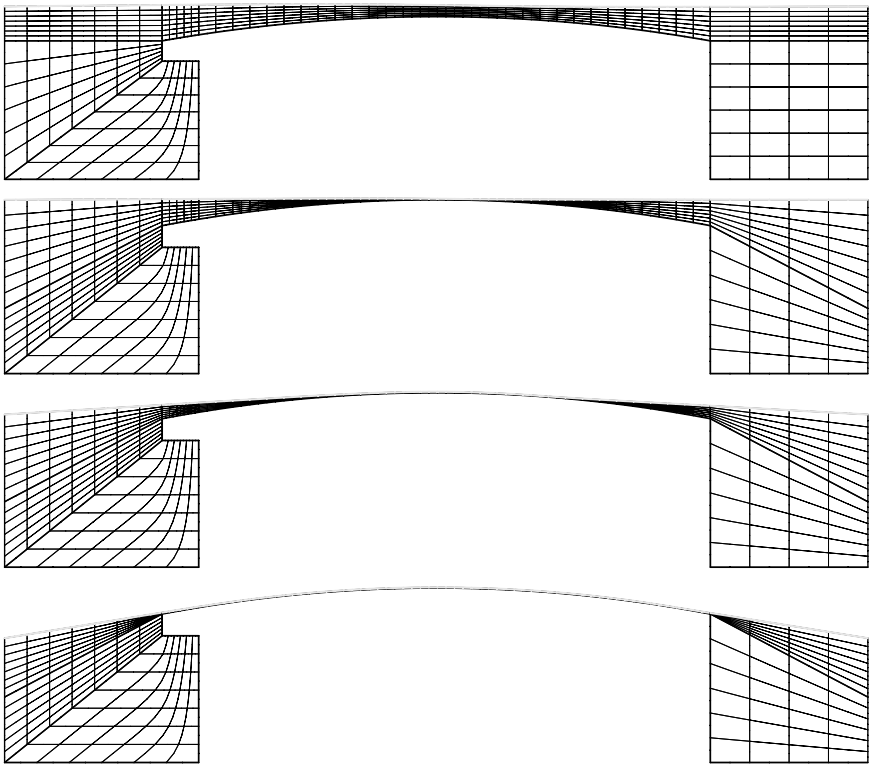

Figure 4: Sequence of solutions as the plate is pushed against the moving web.

3.1. Base Case

As a base for comparison, the theoretical predictions obtained for a web floating over a plate 1.5 m (5 ft) long with a radius of curvature equal to 24.4 m (80 ft) are presented first. The effect of the substrate weight is neglected, i.e., $W = 0$. As a matter of reference, this configuration is denoted as *Plate #1*. Figure 5 illustrates the gap between the web and the plate at different web speeds at a tension of $105\,\text{N/m}$ $(0.6\,\text{lb/in})$ (Tension number τ from 2×10^{-8} up to 3.4×10^{-7}). The position of the plate was fixed at $S^* = 12.7\,\text{cm}$ $(5\,\text{in})$, and the Elasticity number at $N_{ES} = 1.6\times10^{-11}$. The flow can be divided in three regions. The first is the inflow, where the web approaches the plate. Next, there is a region of more or less constant clearance H_0. The last portion, the outflow region, is characterized by an undulation of the web. The minimum gap between the web and the plate $H_{\min}$ occurs close to the exit edge of the plate. For the purpose of determining the heat transfer from the hot plate to the web, the relevant dimension is the almost constant clearance H_0. As the web speed increases, more air is dragged by the moving substrate, raising the clearance H_0.

The effect of the position of the plate (represented by S^*) on the float height is illustrate in Fig.6. The Tension number is $\tau = 2 \times 10^{-8}$ and the Elasticity number is $N_{ES} = 1.6 \times 10^{-11}$. As the tangent point approaches the upstream edge of the plate (S^* falls), the region of uniform gap is extended, separating completely the inflow from the outflow region and the air layer thickness decreases.

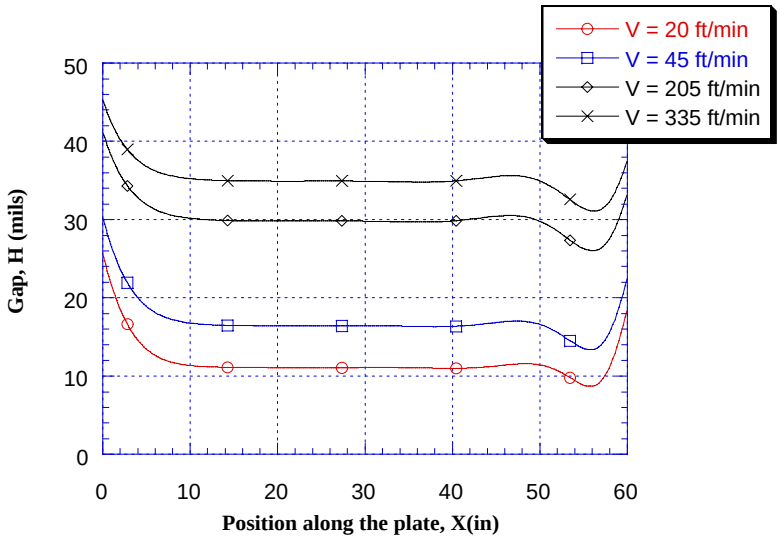

Figure 5: Clearance between the web and Plate #1 at different web speeds (tension number).

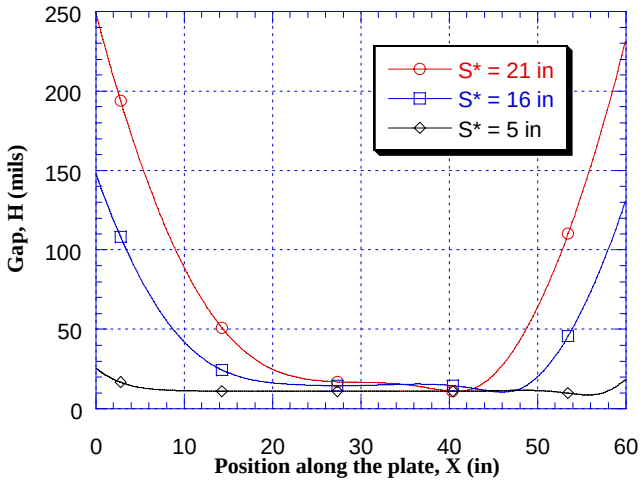

Figure 6: Clearance between the web and Plate #1 at different tangent point positions.

The converging channel at the inflow region leads to a pressure build up in the flowing air, as illustrated in Fig.7. In the uniform gap region, the pressure is almost constant and approximately equal to the tension applied to the web divided by the radius of curvature of the plate, i.e. $P \cong T / R_0$. There is a pure Couette flow. In this class of flow, the channel height is linearly proportional to the flow rate dragged by the web. With the no-leakage hypothesis, the flow rate that goes through the channel is controlled by the combination of Couette and Poiseuille flow in the inlet region, and it follows from elastohydrodynamic theory that the maximum pressure gradient is inversely proportional to the square of the flow rate. The larger the pressure gradient, the more air is rejected and the smaller the flow rate through the gap. As S^* falls, the uniform pressure region is extended closer to the edge of the plate and the adverse pressure gradient at the inlet increases, leading to a smaller air flow rate and consequentially a smaller float height, as it is plain from Fig.6.

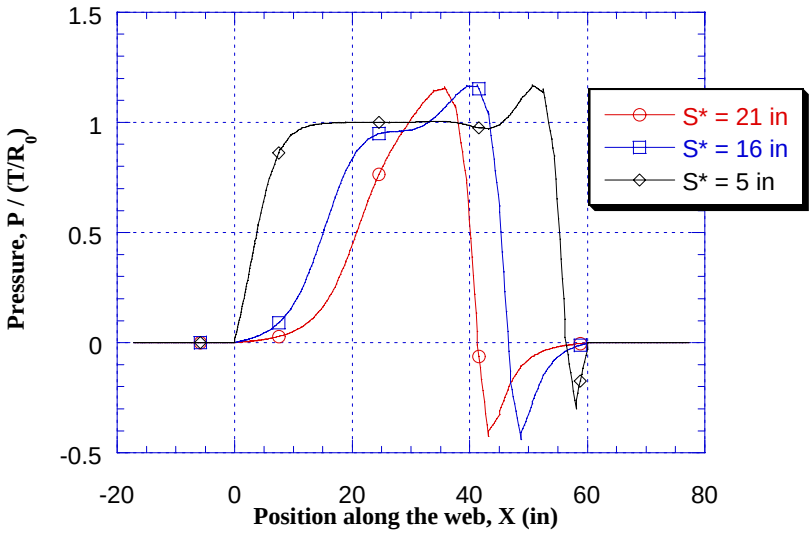

Figure 7: Pressure distribution along the substrate.

3.2. Effect of the geometry of the leading edge on the plate

From the results presented in the previous section, it is clear that the float height can be modified by controlling the pressure gradient at the leading edge of the plate. One way of accomplishing that is to change the position at which the web approaches the plate (S^*). This alternative is not always possible, since changes on the position at which the web approaches the plate may alter the overall web path on the coating line.

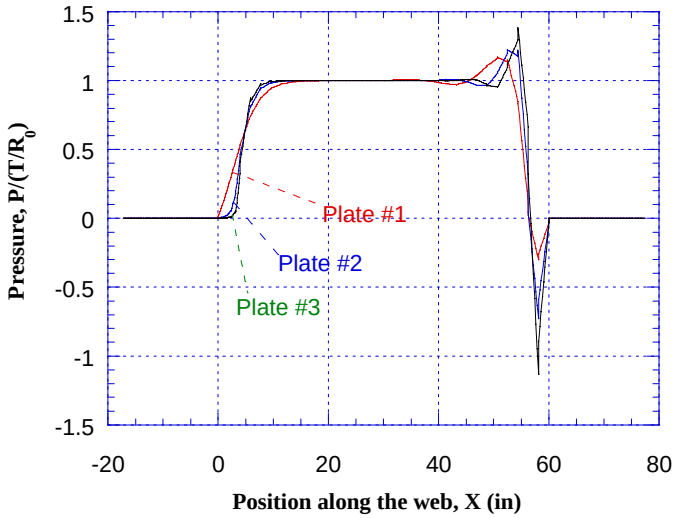

Figure 8: Variation of air layer thickness between web and Plates #1, #2 and #3.

An alternative way is to change the geometry of the leading edge of the radius plate. This is explored in this section by studying the float height of a web traveling over three different plates. They all had a length of $L = 1.5\,\text{m}\ (5\,\text{ft})$ and a main radius of curvature of $R_0 = 22.4\,\text{m}\ (80\,\text{ft})$. The only difference between them was the geometry of the entry section, where the web first approaches the plate. The entry sections of the plates were $10\ \text{cm}\ (4\ \text{in})$ long and also curved. *Plate #1* had an entry radius equal to the rest of the plate, i.e. $R_i = 22.4\,\text{m}\,(80\,\text{ft})$ (this is the geometry analyzed as a base case in the previous section). *Plate #2* had an entry radius equal to $R_i = 1.5\,\text{m}\,(5\,\text{ft})$; and *Plate #3* had an entry radius equal

to $R_i = 0.6\,\text{m}\,(2\,\text{ft})$. The transition between the entry section and the rest of the plate was smooth, i.e. the curved surfaces were tangent at the point (line in three-dimensions) where they met.

Figure 8 shows how the clearance between the web and the plate varies with the tangent point for the three different plates. At large values of S^*, the flow is not affected by the configuration of the entrance region and the predictions of all three plates are virtually the same. As the plate is pushed against the web, and S^* falls, the flow starts to be affected by the geometry of the upstream edge of the plate. At $S^* \le 5\,\text{in}$, the float height is strongly dependent not only on the tangent point but also on the geometry of the entry section. At a fixed value of S^*, the clearance was maximum with *Plate #1* and minimum with *Plate #3*. At $S^* = 5\,\text{in}$, the float height obtained with *Plate #3* is close to half of that obtained with *Plate #1*. The reason is that the pressure gradient at the entrance region with Plate #3 is larger than when the other two plates are used, as illustrated in Fig.9.

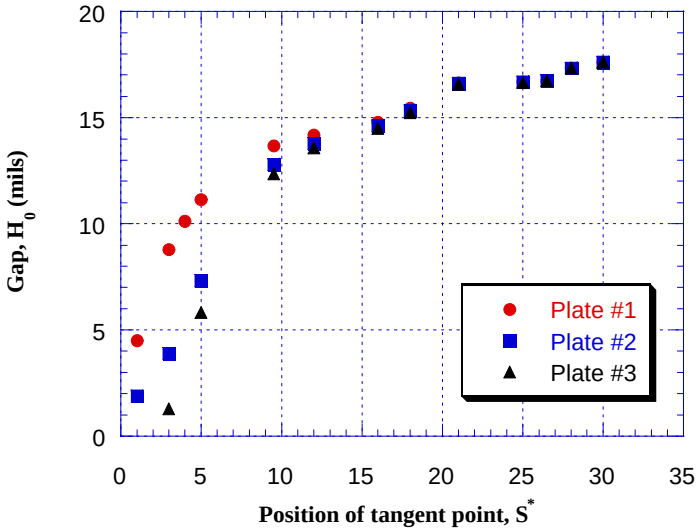

Figure 9: Pressure distribution along the web for Plates #1, #2, and #3.

3.3. Comparison with experimental results

Carvalho and Kolb (1998) performed experiments to measure the air layer thickness between a moving PET substrate and a solid plate with a configuration identical to *Plate #3*. The comparison between theoretical predictions and measured air layer thickness is shown in Fig.10. The agreement over the entire range of tension number is very good, specially at low clearance. At larger air layer thicknesses, the amount of air that leaks through the sides is not negligible, which accounts for the small discrepancy.

4. FINAL REMARKS

It is clear that the theoretical model presented here is able to capture the main physics that governs this situation. The air layer thickness predictions agree well with the available experimental measurements.

The analysis presented here clarified the mechanisms related with this elastohydrodynamic situation. It showed that the clearance between the two surfaces is controlled by the pressure gradient at the entrance section of the channel formed between the web and the plate.

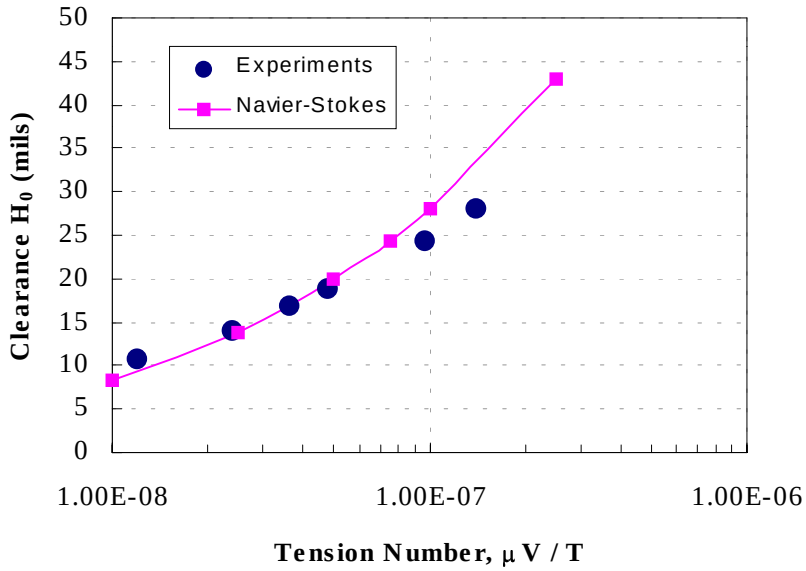

Figure 10: Comparison between experimental measurements and finite element predictions.

REFERENCES

Blok H. and van Rossum J.J. 1953. The Foil Bearing: A New Departure in Hydrodynamic Lubrication. Lubrication Engineering, vol. 9, pp.316-320.

Carvalho M. S. and Kolb W. B. 1998. Elastohydrodynamics of a Moving Web over a Curved Plate: Means of Supporting and Heating a Substrate. 9th International Coating Science and Technology Symposium, pp.9-12.

Carvalho M. S. and Scriven L. E. 1997. Flows in Forward Deformable Roll Coating Gaps: Comparison Between Spring and Plane Strain Model of Roll Cover. Journal of Computational Physics, vol.138(2), pp.449-479.

Eshel A. and Elrod H.G. 1965. The Theory of Infinitely Wide, Perfectly Flexible, Self-Acting Foil Bearing, Journal of Basic Engineering, vol. 87, pp. 831-836.

Eshel A. and Elrod H.G. 1967. Stiffness Effects on the Infinitely Wide Foil Bearing, Journal of Lubrication Technology, vol. 89}, pp.92-97.

Eshel A. 1970. On Controlling the Film Thickness in Self-Acting Foil Bearings, Journal of Lubrication Technology, vol. 92, pp.359-362.

Huelsman G.L. and Kolb W.B. 1997. Coated Substrate Drying System. U.S. Patent No. 5,694,701, Minnesota Mining and Manufacturing Company.

Kistler S.F. and Scriven L.E. 1983. Coating Flows. Computational Analysis of Polymer Processing (Eds. J.R.A. Pearson and S.M. Richardson), Applied Science Publishers, London, pp.243.

Kistler S.F. and Scriven L.E. 1984. Coating flow theory by finite element and asymptotic analysis of the Navier-Stokes system. International Journal for Numerical Methods in Fluids, vol. 4, pp.207.

Kolb W.B, and Huelsman G.L. 1998. Gap Drying: An Overview. 9th International Coating Science and Technology Symposium, pp.209-212.

Licht L. 1968. An Experimental Study of Elastohydrodynamic Lubrication of Foil Bearings, Journal of Lubrication Technology, vol. 90, pp.199-220.

Sakinger P.A., Schunk P.R. and Rao R.R. 1996. A Newton-Raphson Pseudo-Solid Domain Mapping Technique for Free and Moving Boundary Problems: A Finite Element Implementation. Journal of Computational Physics, vol. 125, pp.83-103.